Nuclear Science and Techniques **24** (2013) S010312

Pulse radiolysis and laser flash photolysis study of balofloxacin

XU Yulie[1,2] LIU Yancheng[1,2] LI Haixia[1,2] ZHANG Peng[1] TANG Ruizhi[1,2]
CAO Xiyan[3] WANG Wenfeng[1,*]

[1]*Shanghai Institute of Applied Physics, Chinese Academy of Sciences, Shanghai 201800, China*

[2]*Graduate University of Chinese Academy of Science, Beijing 100049, China*

[3]*School of Chemistry and Chemical Engineering, Hunan University of Science and Technology, Xiangtan 411201, China*

Abstract Pulse radiolysis studies of the reactions between balofloxacin (BFX) and e_{aq}^-, hydroxyl radical ($^{\cdot}OH$), and $N_3^{\cdot}$ were carried out to investigate the photosensitive toxicity of BFX. The BFX radical anion formed in the reaction of BFX with e_{aq}^- was located at 380 nm. The transient species formed in the reaction of BFX with $^{\cdot}OH$ radical were located in the region of 370 nm to 580 nm, with a maximum λ_{max} at 390 nm. The BFX radical cation was obtained by reacting BFX with $N_3^{\cdot}$, and showed an absorption band at around 365 nm. The UV-Vis absorption of the BFX was found to be clearly dependent on pH. The pK_a value of BFX was estimated to be 6.0±0.2. Under neutral conditions, the rate constants of BFX reacting with $N_3^{\cdot}$ and e_{aq}^- were determined to be 1.3×10^{10} $dm^3\cdot mol^{-1}\cdot s^{-1}$ and 1.4×10^{10} $dm^3\cdot mol^{-1}\cdot s^{-1}$, respectively.

Key words Balofloxacin, Pulse radiolysis, Laser flash photolysis, Fluoroquinolones

1 Introduction

Fluoroquinolones (FQs), which have a wide antibacterial spectrum, are some of the most successful types of antibiotic agents, and are also a new and potent orally-absorbed antimicrobial agent. The pharmacological action of FQs is derived from the primary bacterial target, the enzyme deoxyribonucleic acid gyrase[1]. Although FQs play a crucial part in antibacterial therapy, their side effects, such as phototoxicity and photocarcinogenic activity, have attracted the attention of researchers[2–5], as the transient species of some FQs occure in the neutral aqueous media[6–9].

FQs derivatives are widely used as antibiotics because of their high efficiency. Over the past decade, a number of studies concerning the phototoxicity of FQs have identified their main photoprocess as heterolytic defluorination. The structure-side effect of newly-developed FQs has also been evaluated. Photochemists have shown great interest in the photodefluorination[10–19] of many FQs, which is an uncommon process in the broad area of fluoroaromatic photochemistry, as well as an unexpected reaction involving fluoroaromatics resulting from the power of the aromatic C-F bond (dissociation energy *ca* 120 $kcal\cdot mol^{-1}$)[14].

This paper presents an overview of balofloxacin (BFX) (Fig.1), a new, fourth-generation synthetic antibacterial FQ agent. BFX is well tolerated, and its chief excretion route is renal[20]. The effects of pH and buffer solution on the photochemical features of BFX have been researched using the fluorescent spectrometry method[21,22].

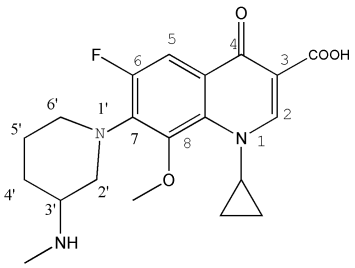

Fig.1 Structure of BFX.

Supported by National Natural Science Foundation of China (No 21173252)

* Corresponding author. *E-mail address:* xuyulie@sinap.ac.cn; wangwenfeng@sianp.ac.cn

Received date: 2012-12-31

This study investigates the photochemical and photophysical properties of BFX in an aqueous media using the UV-Vis, the fluorescence measurement, the laser flash photolysis, and the nanosecond pulse radiolysis techniques.

The pulse radiolysis study investigated the reactions of BFX with hydroxyl radical ($^{\cdot}OH$), $N_3^{\cdot}$, and e_{aq}^-. The transient absorption and kinetic rate constants were obtained, and the pH dependence of BFX was investigated. Photosensitive damage to biological molecules could be investigated more effectively by studying the nature of BFX radicals.

2 Materials and methods

2.1 Materials

Balofloxacin was purchased from J&K Chemical Ltd and used without further purification. NaOH, $HClO_4$, and phosphate (analytic grade reagent) were obtained in a commercial manner and used as received. Water was purified through a Millipore Milli-Q system. The pH of the solutions was measured by a glass electrode.

2.2 Laser flash photolysis

A neodymium-doped yttrium aluminum garnet, Nd: Y3Al5O12 (Nd:YAG) laser system was used to conduct laser flash photolysis experiments. This system featured a Q-switched 1 J pulse energy with a 12 ns pulse width as the excitation source. The harmonics were divided by using a beam splitter. The samples under investigation were contained in a quartz cell and were replaced after each laser pulse. The analyzing beam was generated by a xenon lamp and passed through the samples at a right angle to the laser beam. The wavelengths of the monitoring light were then dispersed by a monochromator and passed into a photomultiplier. The detector was linked to an automatic back-off box that allowed changes in transmittance to be observed by feeding back an equal and opposite signal to the detector anode current prior to laser pulse, thus keeping anode current near zero.

The photomultiplier (Hamamatsu R925) output was displayed on a digitizing oscilloscope. Data was handled on a personal computer using software developed in-house Back-off and energy meter readings were digitized using an analogue-to-digital converter connected to a DI-AN data acquisition system. Data were acquired and handled by repeating the above procedure at successive wavelengths.

2.3 Pulse radiolysis

The nanosecond pulse radiolysis experiments were conducted using a 10 MeV linear accelerator, which transmitted an electron pulse with using duration of 8 ns. The dosimetry of the electron pulse was determined in a previous paper[23] using a thiocyanate dosimeter using G $[(CNS)_2^{\cdot-}] = 5.8$ in 1×10^{-4} mol·dm^{-3} KCNS saturated with N_2O by taking $\varepsilon_{480\ nm}$=7 600 dm^3·mol^{-1}·s^{-1} for $(CNS)_2^{\cdot-}$. The details of the setup and operational conditions were introduced and the dose per electron pulse was set at 10 Gy.

A xenon lamp was used as the light source for the detection. The electron pulse and the analyzing light beam passed perpendicularly through the quartz cell. The transmitted light then entered the monochromator with an R955 photomultiplier. The output signal from the leCroy wavemaster 8600A digital oscillograph was entered into a personal computer for further analysis.

Tert-butanol was used to scavenge the leftover $^{\cdot}OH$, and e_{aq}^- to create a reducing environment. The sample solution was also saturated with N_2O prior to pulse radiolysis to produce an almost uniform $^{\cdot}OH$ radical oxidizing solution environment where e_{aq}^- was converted to $^{\cdot}OH$ based on the reactions below:

$$H_2O+\gamma+e^-\rightarrow e_{aq}^-,\ H,\ ^{\cdot}OH,\ H_2,\ H_2O_2,\ HO_2 \quad (1)$$

$$^{\cdot}OH + \text{tert-BuOH} \rightarrow \text{tert-BuO}^{\cdot} + H_2O \quad (2)$$

$$k = 5.1\times10^8\ \text{dm}^3\cdot\text{mol}^{-1}\cdot\text{s}^{-1}$$

$$e_{aq}^- + N_2O + H_2O \rightarrow {}^{\cdot}OH + OH^- + N_2 \quad (3)$$

$$k = 8.7\times10^9\ \text{dm}^3\cdot\text{mol}^{-1}\cdot\text{s}^{-1}$$

The following reaction is applied to produce quantitatively secondary one-electron oxidants ($N_3^{\cdot}$). Subsequent results of these secondary oxidants with BFX caused the emergence of one-electron oxidized BFX transient types.

$$^{\cdot}OH + N_3^- \rightarrow N_3^{\cdot} + OH^- \quad (4)$$

$$k = 2\times10^{10}\ \text{dm}^3\cdot\text{mol}^{-1}\cdot\text{s}^{-1}$$

3 Results and discussion

BFX is an effective antibiotic that allows phototoxicity and photoionization reactions to take place easily. It is

therefore necessary to investigate the reduction and oxidation products of BFX, which may prove useful in relative pathological studies.

3.1 Absorption and emission properties

As shown in Fig.2, the UV-Vis absorption spectroscopy shows two absorption peaks in the range of 260 nm to 400 nm. The short-wave absorption band (260 nm to 310 nm) is chiefly caused by the electron transition of aromatic nuclei from π to π*[24]. The long-wave absorption band (310 nm to 380 nm) is chiefly caused by electron transition from *n* to π* (HOMO-LUMO)[25]. As pH increases, blue shift occurs from 293 nm to 285 nm in the maximum absorption peak. Simultaneously, red shift appears in the long-wave absorption band, and the absorbance is gradually reinforced as pH increases. Two obvious absorptive points can be observed at 325 nm and 350 nm. In the range of pH 3 to pH 10, the proton balance process of BFX only involves proton dissociation of the carboxyl group. Scheme 1 shows four proton binding points in the structure of BFX. However, the current experiment does not attempt to determine which proton binding point is protonated. From these curves, a pK_a value of 6.0±0.2 is deduced, corresponding to the pK_a for the dissociation of the carboxylic of the molecule. Thus, at a neutral pH, the predominant structure is a neutral form.

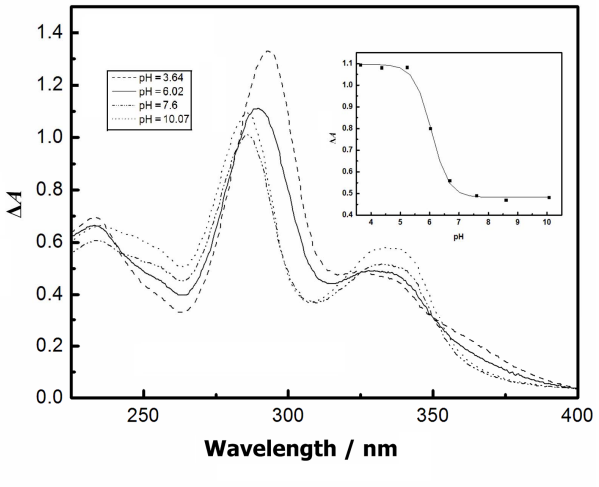

Fig.2 Absorption spectra of BFX (2×10^{-5} mol·dm^{-3}) in aqueous buffered solution as a function of pH Inset: variation of 278 nm absorption against different pH values.

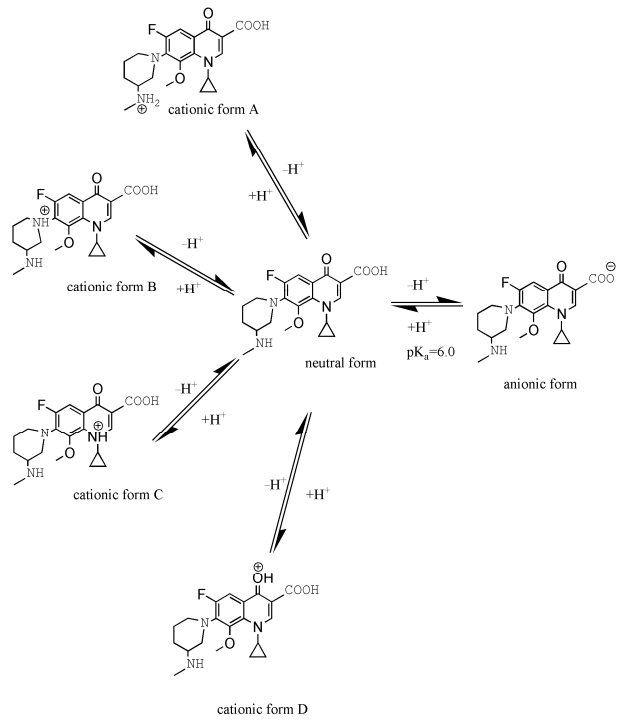

Scheme 1 Equilibria between protonated forms of BFX.

Figure 3 shows the obvious effects of pH changes on BFX fluorescence, with the intensity of the BFX fluorescence at its peak when pH=7.53.

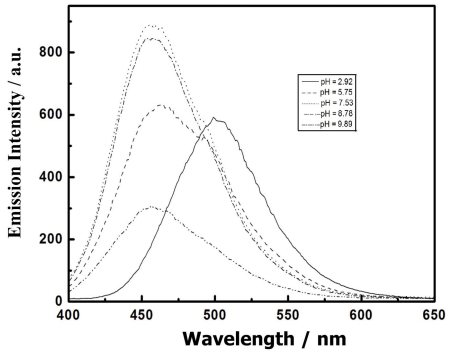

Fig.3 Fluorescence emission spectra of aqueous BFX solution recorded at different pH values. Inset: variation of the fluorescence quantum yield with pH (λ_{exc}= 355 nm).

The maximum emission wavelength of the BFX fluorescence has a blue shift, and the intensity of the fluorescence gradually increases as the pH rises from 2.92 to 7.53. When pH exceeds 7.53, the intensity of the maximum emission wavelength of the fluorescence decreases as the pH rises. However, after the fluorescence intensity gradually attenuates and pH exceeds 12, the BFX fluorescence can hardly be observed. The fluorescence spectrum of BFX at pH 7.53 shows a broad band at around 460 nm. The

presence of both an electron-donating amino group and an electron-withdrawing F substituent can explain this shift, which results in the $\pi\rightarrow\pi^*$ excited state to hold some internal charge transfer character[26,27]. This effect could be the result of deprotonation of BFX at a high pH, as this deprotonation renders a lone pair of electrons, which are available to participate in an intermolecular electron transfer. Therefore, a very efficient pathway is established as a result of the deactivation of the singlet excited state[28].

3.2 Laser flash photolysis

Figure 4 shows the transient absorption spectra, obtained via the 355nm laser flash photolysis, of air, N_2O, N_2, and O_2^- saturated BFX (1×10^{-4} mol·dm^{-3}) aqueous solutions containing 2×10^{-3} mol·dm^{-3} phosphate buffer (PB, pH 7.0).

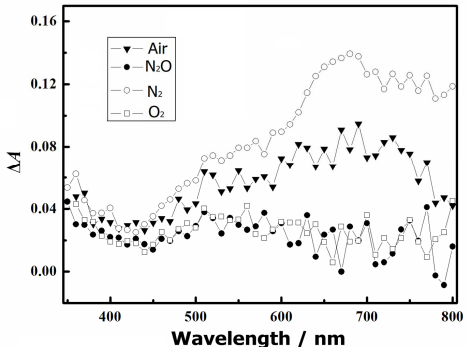

Fig.4 Absorption spectrum of the transient species of BFX (1×10^{-4} mol·L^{-1}) produced from 355 nm laser flash photolysis in neutral aqueous solutions (PB 2×10^{-3} mol·dm^{-3}, pH 7.0) saturated with air (-▼-), N_2O (-●-), N_2 (-○-), and O_2 (-□-).

As shown in Fig.3, the λ_{max} is located at 700 nm. The absorption around 700 nm decreases when the neutral aqueous solutions saturated with N_2O and O_2 At 700 nm, as O_2 concentration increases, the absorption peak of e_{aq}^- decreases, which results from the reaction of e_{aq}^- and O_2, and then produces $O_2^{-\cdot}$ (Reaction 5) At the same time, saturated with N_2O, the absorption of e_{aq}^- almost disappears, because e_{aq}^- is scavenged by N_2O, producing $^{\cdot}OH$ (Reaction 3). The transient species with characteristic absorption at 360 nm may be from BFX radical cation ($BFX^{+\cdot}$) (Reaction 6) as the BFX reacts with the oxidative free radicals $O_2^{-\cdot}$ and $^{\cdot}OH$. Intensive photoionization evidently occurred, based on the formation of hydrated electrons. Thus, the photoionization process of BFX has been confirmed.

$$e_{aq}^- + O_2 \rightarrow O_2^{-\cdot} \quad (5)$$

$$^{\cdot}OH + BFX \rightarrow BFX^{+\cdot} + OH^- \quad (6)$$

By using N_2O to remove e_{aq}^- absorption[29], pure $^3BFX^*$ absorption can be observed at 720 nm. Finally, the transient absorbance of pure e_{aq}^- can be obtained by subtracting that obtained in N_2O saturated system from that in N_2 saturated system.

As shown in Fig.5, there is a perfect line between the quantum yield of hydrated electron recorded at 720 nm and the intensities of laser pulse, which means the photoionization of BFX in neutral aqueous solution is single photon process similar to moxifloxacin[30] and ofloxacin[28,31]. This result contrasts with those of other FQs, whose photoionizations have been found to be bi-photonic[32]. However, the hydrated electron should react with BFX to form BFX anion radicals. Obvious, relatively long-life instantaneous absorption is observed at 380 nm, which will be confirmed in following experimental pulse radiolysis with BFX.

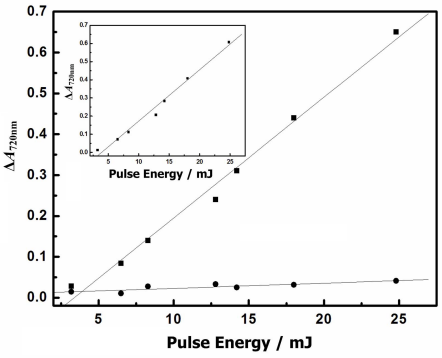

Fig. 5 Plot of the transient absorbance recorded at 720 nm against the intensities of laser pulse obtained in 355nm laser flash photolysis of BFX in neutral aqueous solutions saturated with N_2 (-■-) and N_2O (-●-) (50 ns after the pulse) Inset: the difference between the ΔA_{720} nm in N_2 and N_2O aganst the intensities of laser pulse.

$$\Delta\Delta A_{720nm} = \Delta\Delta A_{720nm}(N_2) - \Delta\Delta A_{720nm}(N_2O) \quad (7)$$

3.3 Pulse radiolysis

3.3.1 Reaction of BFX with e_{aq}^-

As shown in Fig.6, a transient absorption spectrum could be obtained in pulse radiolysis of neutral aqueous solution containing 1×10^{-4} mol·dm^{-3} BFX with additive of 0.1 mol·dm^{-3} tert-butanol as scavenger of OH radical. Under these conditions, hydroxyl radicals are removed by the tert-butanol and only e_{aq}^- remained. According to Reaction 8, the transient products in this case are mainly BFX anion

radicals ($BFX^{\cdot-}$). Simultaneously, the reduction of $BFX^{\cdot-}$ corresponds with pseudo-first order kinetics and a rate constant of 1.4×10^{10} $dm^3\cdot mol^{-1}\cdot s^{-1}$ has been obtained with various concentration of BFX.

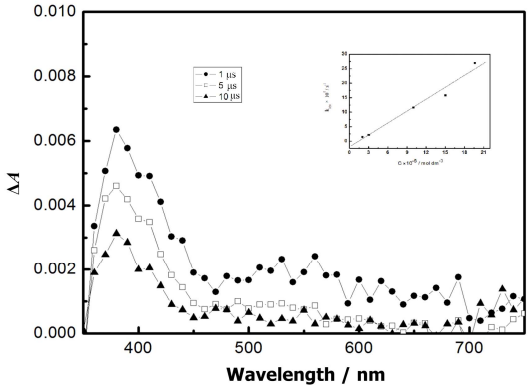

Fig.6 Transient difference absorption spectra observed at 1 μs (-●-), 5 μs (-□-) and 10 μs (-▲-) after pulse radiolysis of N_2-saturated neutral aqueous solution containing 0.1 mol dm^{-3} tert-butanol. Inset: plot of the observed rates of BFX with e_{aq}^- as a function of BFX concentration at 380 nm.

$$BFX + e_{aq}^- \rightarrow BFX^{\cdot-} \quad (8)$$

3.3.2 Oxidation of BFX by $N_3^{\cdot}$

The reactions between the azide radical $N_3^{\cdot}$ and BFX are initially studied to investigate the reactions of BFX with $^{\cdot}OH$ in depth, because the latter reactions may emerge by means of additional redox reactions or hydrogen abstraction. By contrast, BFX can only react with $N_3^{\cdot}$ via electron transfer form to $BFX^{\cdot+}$. In the pulse radiolysis of N_2O-saturated aqueous solution the hydrated electron is transferred into $^{\cdot}OH$, which makes N_3^- oxidized to form $N_3^{\cdot}$. Afterwards, the BFX is oxidized accordingly by $N_3^{\cdot}$ via electron transfer reactions. As shown in Fig.7, the species with maximum absorption at 365 nm should be assigned to be $BFX^{\bullet+}$, and the rate constant for the reaction as shown in function (9) is estimated to be 1.3×10^{10} $dm^3\cdot mol^{-1}\cdot s^{-1}$.

$$N_3^{\cdot} + BFX \rightarrow N_3^- + BFX^{\cdot+} \quad (9)$$

3.3.3 Reaction of BFX with $^{\cdot}OH$

Reactions between BFX and $^{\cdot}OH$ may manifest themselves in various ways: redox reactions occur with the emergence of BFX radical cations, addition reactions appear with the development of additional products, and hydrogen abstraction reactions happen with the occurrence of BFX neutral radicals (Reactions 10 to 12). However, the reaction between subsequent products of BFX attacked by $\cdot OH$ and biologic materials is complicated, which needs to be explored further (Fig.8).

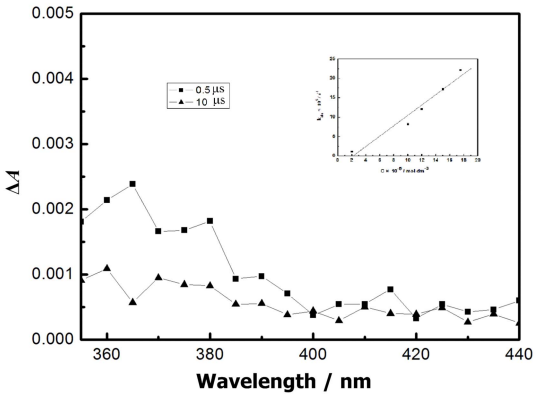

Fig.7 Transient absorption spectra recorded at 0.5 μs (-■-) and 10 μs (-▲-) after electron pulse subjecting N_2O– saturated neutral aqueous solution containing 0.2 mM BFX and 0.1 M NaN_3. Inset: plot of the observed forming rates of $BFX^{\cdot+}$ for reaction of BFX with $N_3^{\cdot}$ as a function of BFX concentrations observed at 365 nm.

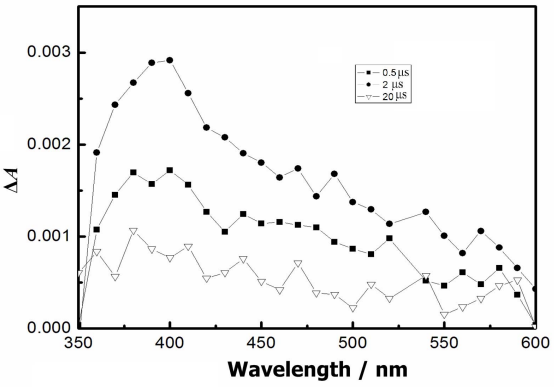

Fig.8 Transient absorption spectra observed at 0.5 μs (-■-), 2 μs (-●-) and 20 μs (-▽-) in the pulse radiolysis of N_2O-saturated neutral aqueous solution containing 0.2 mM BFX.

$$BFX + \cdot OH \rightarrow BFX^{\cdot+} + OH^- \quad (10)$$

$$BFX + \cdot OH \rightarrow BFX\text{-}OH^{\cdot} \quad (11)$$

$$BFX + \cdot OH \rightarrow BFX(-H)^{\bullet} + H_2O \quad (12)$$

4 Conclusion

The present work provided systematic results of the photochemical and photophysical properties of BFX. The p*K*a value was determined by studying the UV-Vis spectra of BFX. It was found that there was an obvious effect on BFX fluorescence at different pH. The photoionization process of BFX was studied using laser flash photolysis, and the reactions of BFX with $^{\cdot}OH$, e_{aq}^-, and $N_3^{\cdot}$ were investigated via pulse radiolysis. As the biological consequences of the

reactions of such transient species with biomolecules are unclear, it needs more exploration to understand relative mechanism.

References

1 Domagala J M, Hanna L D, Heifetz C L, *et al.* J Med Chem 1986, **29:** 394–404.

2 Wolfson J S, Hooper D C. Clin Microbiol Rev, 1989, **2:** 378–424.

3 Martinez L, Chignell C F. J Photoch Photobio B, 1998, **45:** 51–59.

4 Cheng L L, Zhao P, Wang M, *et al.* Acta Phys-Chim Sin, 2009, **25:** 25–29.

5 Lhiaubet-Vallet V, Bosca F, Miranda M A. Photochem Photobiol, 2009, **85:** 861–868.

6 Van Doorslaer X, Demeestere K, Heynderickx P M, *et al.* Appl Catal B-Env, 2011, **101:** 540–547.

7 Mella M, Fasani E, Albini A. Helv Chim Acta, 2001, **84:** 2508–2519.

8 Ling X, Zhong W Y, Huang Q, *et al.* J Photoch Photobio B, 2008, **93:** 172–176.

9 ElWalily A F M, Belal S F, Bakry R S. J Pharmaceut Biomed, 1996, **14:** 561–569.

10 Fasani E, Mella M, Caccia D, *et al.* Chem Commun, 1997, 1329–1330.

11 Martinez L J, Li G, Chignell C F. Photochem Photobiol, 1997, **65:** 599–602.

12 Fasani E, Negra F F B, Mella M, *et al.* J Org Chem, 1999, **64:** 5388–5395.

13 Fasani E, Rampi M, Albini A. J Chem Soc Perk T2. 1999, 1901–1907.

14 Albini A, Monti S. Chem Soc Rev, 2003, **32:** 238–250.

15 Cuquerella M C, Bosca F, Miranda M A. J Org Chem, 2004, **69:** 7256–7261.

16 Fasani E, Mella M, Albini A. Eur J Org Chem, 2004, 5075–5082.

17 Cuquerella M C, Miranda M A, Bosca F. J Phys Chem A, 2006, **110:** 2607–2612.

18 Cuquerella M C, Miranda M A, Bosca F. J Phys Chem B, 2006, **110:** 6441–6443.

19 Fasani E, Monti S, Manet I, *et al.* Org Lett, 2009, **11:** 1875–1878.

20 Kozawa O, Uematsu T, Matsuno H, *et al.* Antimicrob Agents Ch, 1996, **40:** 2824–2828.

21 Qi X J, Wang J X, Liu Z R. Chin J Analyt Chem, 2006, **34:** 1047–1047.

22 Yan Z Y, Shao X F, Jiang X M, *et al.* Spectroscopy Spectra Anal, 2006, **26:** 1494–1498.

23 Yao S D, Sheng S G, Cai J H, *et al.* Radiat Phys Chem, 1995, **46:** 105–109.

24 Agrawal N, Ray R S, Farooq M, *et al.* Photochem Photobiol, 2007, **83:** 1226–1236.

25 Carlucci G. J Chromatogr A, 1998, **812:** 343–367.

26 Navaratnam S. J Claridge Photochem Photobiol, 2000, **72:** 283–290.

27 Neugebauer U, Szeghalmi A, Schmitt M, *et al.* Spectrochem Acta A, 2005, **61:** 1505–1517.

28 Lorenzo F, Navaratnam S, Edge R, *et al.* Photochem Photobiol, 2009, **85:** 886–894.

29 Buxton G V, Greenstock C L, Helman W P, *et al.* J Phys Chem Ref Data, 1988, **17:** 513–886.

30 Lorenzo F, Navaratnam S, R Edge, *et al.* Photochem Photobiol, 2008, **84:** 1118–1125.

31 Lian N, Zhao H C, Sun C Y, *et al.* Chem J Chin U, 2002, **23:** 564–566.

32 Monti S, Sortino S. Photoch Photobio Sci, 2002, **1:** 877–881.